
Efficient prediction of 3D electron densities using machine learning

Mihail Bogojeski*¹, Felix Brockherde*^{1,2}, Leslie Vogt-Maranto*³, Li Li^{†4}, Mark E. Tuckerman^{3,5,6}, Kieron Burke^{4,7}, and Klaus-Robert Müller^{1,8,9}

¹Machine Learning Group, Technische Universität Berlin, Marchstr. 23, 10587 Berlin, Germany

²Max-Planck-Institut für Mikrostrukturphysik, Weinberg 2, 06120 Halle, Germany

³Department of Chemistry, New York University, New York, NY 10003, USA

⁴Departments of Physics and Astronomy, University of California, Irvine, CA 92697, USA

⁵Courant Institute of Mathematical Science, New York University, New York, NY 10003, USA

⁶NYU-ECNU Center for Computational Chemistry at NYU Shanghai, 3663 Zhongshan Road North, Shanghai 200062, China

⁷Department of Chemistry, University of California, Irvine, CA 92697, USA

⁸Department of Brain and Cognitive Engineering, Korea University, Anam-dong, Seongbuk-gu, Seoul 02841, Korea

⁹Max-Planck-Institut für Informatik, Stuhlsatzenhausweg, 66123 Saarbrücken, Germany

Abstract

The Kohn–Sham scheme of density functional theory is one of the most widely used methods to solve electronic structure problems for a vast variety of atomistic systems across different scientific fields. While the method is fast relative to other first principles methods and widely successful, the computational time needed is still not negligible, making it difficult to perform calculations for very large systems or over long time-scales. In this submission, we revisit a machine learning model capable of learning the electron density and the corresponding energy functional based on a set of training examples. It allows us to bypass solving the Kohn-Sham equations, providing a significant decrease in computation time. We specifically focus on the machine learning formulation of the Hohenberg-Kohn map and its decomposability. We give results and discuss challenges, limits and future directions.

1 Introduction

The electron density $n(\mathbf{r})$ is one of the fundamental properties of atomistic systems. According to the first Hohenberg-Kohn theorem of density functional theory (DFT) the electron density uniquely determines the ground state properties of an atomistic system [1]. Kohn-Sham density functional theory [2] (KS-DFT) provides a relatively efficient framework for calculating the electronic energy, making it one of the most popular electronic structure methods across a wide array of fields [3].

Recently, there has been an increase in the application of machine learning (ML) methods to various problems regarding atomistic systems[4]. Such machine learning models have been applied for the prediction of properties of molecules and materials by learning from a large database of reference calculations [5–13], performing molecular dynamics (MD) by learning the potential energy surfaces/force fields for particular molecules [14–21], and in few cases for the prediction of electron densities as a means of performing electronic structure calculations in the DFT framework without

*Contributed equally.

[†]Currently at Google AI

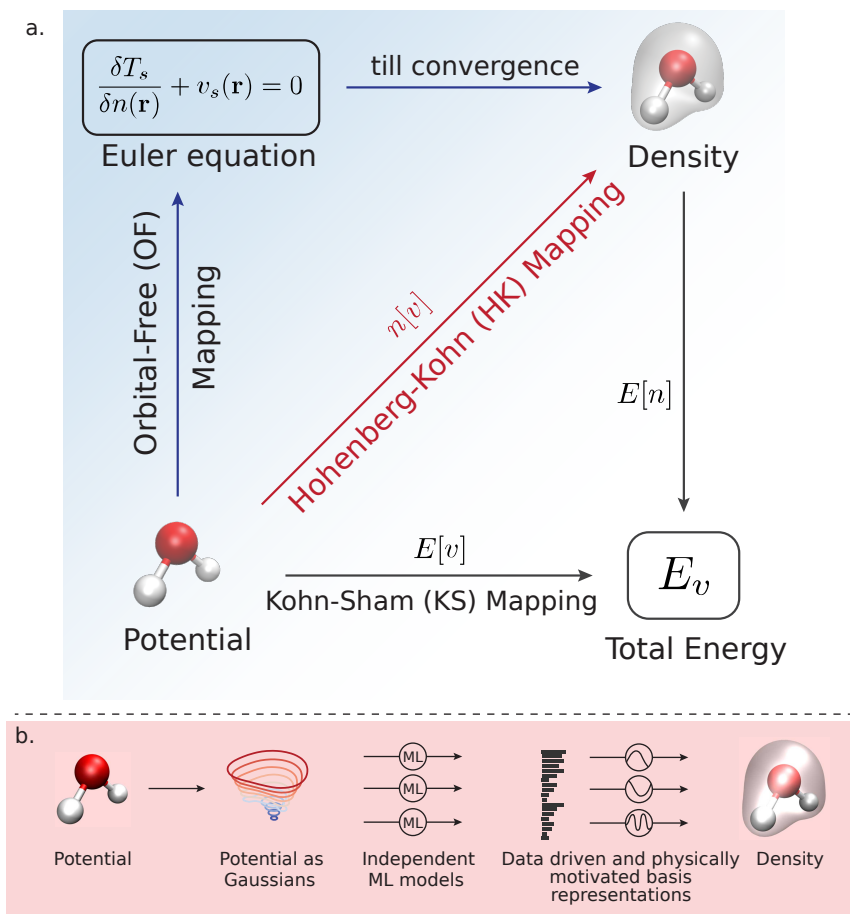


Figure 1: **Overview of the ML-HK map** **a.** General overview of machine learning models for the total energy. The bottom arrow represents $E[v]$, a conventional electronic structure calculation, i.e., KS-DFT. The ground state energy is found by solving KS equations given the external potential, v . $E[n]$ is the total energy density functional. The red arrow is the HK map $n[v]$ from external potential to its ground state density. **b.** How the machine learning Hohenberg-Kohn (ML-HK) map makes predictions. The molecular geometry is represented by Gaussians; many independent Kernel Ridge Regression models predict each basis coefficient of the density. We analyze the performance of data-driven (ML) and common physical basis representations for the electron density. Figure adapted from Brockherde et al. [24].

solving the expensive Kohn-Sham equations [22–28]. These machine learning methods are often able to predict properties of atomistic systems or perform MD simulations at a similar accuracy to DFT calculations while requiring a fraction of the computation costs, which could potentially allow computational scientists to examine larger systems and/or longer time-scales.

In this submission we will revisit a paper by Brockherde et al. [24], which deals with bypassing the Kohn-Sham equations by first learning the Hohenberg-Kohn (HK) map from the one-body potential $v(\mathbf{r})$ to the electron density $n(\mathbf{r})$ of an atomistic system. Subsequently a second model is used to learn the energy functional from the predicted density to the total energy of the system. This way, the model provides both approximations to the electron density as well as accurate potential energy surfaces suitable for molecular dynamics simulations of small atomistic systems.

Here we will focus on the machine learning approach used, especially for the Hohenberg-Kohn map, and explain in a more didactic manner how this approach enables us to predict the density using multiple independent models, making the learning problem much simpler.

2 Methods

2.1 Kohn-Sham density functional theory (KS-DFT)

The KS-DFT computational electronic structure method is based on the Hohenberg-Kohn theorem [1] which establishes the unique correspondence between the potential and electron density, i.e. at most one potential can produce a given ground-state electron density. KS-DFT can thus be used to calculate various properties of many-body atomistic systems using functionals of the electron density.

The KS-DFT scheme models a fictitious system of non-interacting electrons whose density is the same as the real one, thereby avoiding direct calculation of the many-body effects [2]. The accuracy of KS-DFT is limited by the accuracy of the used approximation to the unknown exchange-correlation energy, whereas the main computational bottleneck is computing the solution of the KS equations describing the non-interacting orbitals, which has a complexity of $\mathcal{O}(n^3)$.

All 3D DFT calculations used in this submission are performed with the Quantum ESPRESSO software [29], using the PBE exchange-correlation functional [30] and projector augmented waves (PAWs) [31, 32] with Troullier-Martin pseudization for describing the ionic cores [33]. All molecules are simulated in a cubic box ($L = 20$ bohr) with a wave function cutoff of 90 Ry.

2.2 Kernel ridge regression (KRR)

KRR [34] is a machine learning method for non-linear regression. Non-linearity is achieved by incorporating the kernel trick into linear ridge regression, which finds the optimal linear mapping from the input to the labels under ℓ_2 regularization. Let $\mathbf{x}_1, \dots, \mathbf{x}_M \in \mathbb{R}^d$ be the training data points and let $\mathbf{Y} = [\mathbf{y}_1, \dots, \mathbf{y}_M]^T$ be their respective labels. The KRR model for a new input sample \mathbf{x}^* is then given by:

$$\mathbf{y}^* = \sum_{i=1}^M \alpha_i k(\mathbf{x}^*, \mathbf{x}_i), \quad (1)$$

where k is a kernel function and $\boldsymbol{\alpha} = [\alpha_1, \dots, \alpha_M]^T$ are the model weights. The model weights are obtained by solving the following optimization problem:

$$\min_{\boldsymbol{\alpha}} \left\{ \sum_{i=1}^m \left| \mathbf{y}_i - \sum_{j=1}^m \alpha_j k(\mathbf{x}_i, \mathbf{x}_j) \right|^2 + \lambda \boldsymbol{\alpha} \mathbf{K} \boldsymbol{\alpha} \right\} \quad (2)$$

where λ is a regularization parameter and \mathbf{K} is the kernel matrix with $\mathbf{K}_{ij} = k(\mathbf{x}_i, \mathbf{x}_j)$. The analytical solution to the minimization problem is then given by

$$\boldsymbol{\alpha} = (\mathbf{K} + \lambda \mathbf{I})^{-1} \mathbf{Y}. \quad (3)$$

Here we use the Gaussian (radial basis function) kernel

$$k(\mathbf{x}, \mathbf{x}') = \exp\left(-\frac{\|\mathbf{x} - \mathbf{x}'\|^2}{2\sigma^2}\right), \quad (4)$$

where the kernel width σ is a model parameter that needs to be tuned using cross-validation.

2.3 Machine learning Hohenberg-Kohn (ML-HK) map

The ML-HK map was introduced in a paper by Brockherde et al. [24] as a way to avoid minimizing the total energy using gradient descent, requiring the calculation of gradient the kinetic energy model, which is often unstable due to missing information about direction outside of the data manifold [35].

As an alternative, the ML-HK map is a multivariate machine learning model that directly learns the electron density $n(\mathbf{r})$ as a functional of the potential $v(\mathbf{r})$, thereby completely bypassing the need for calculating the kinetic energy gradient (see Figure 1a).

As a first step, we model the potential of a system using an artificial Gaussians potential, which is calculated as:

$$v(\mathbf{r}) = \sum_{\alpha=1}^{N^a} Z_{\alpha} \exp\left(\frac{-\|\mathbf{r} - \mathbf{R}_{\alpha}\|^2}{2\gamma^2}\right), \quad (5)$$

where \mathbf{R}_α is the position and Z_α the nuclear charge of the α -th atom. The resulting artificial potential is evaluated on a 3D grid around the molecule and is used in this form as a descriptor for the ML model. Cross-validation can be used to optimize the width γ of the artificial potential as well as the spacing Δ of the grid. We will use \mathbf{v} to denote vector representation of the potential evaluated on a 3D grid.

Using this artificial potential as the descriptor, a naive formulation of the ML-HK map would be

$$n^{\text{ML}}[\mathbf{v}](\mathbf{r}) = \sum_{i=1}^M \beta_i(\mathbf{r})k(\mathbf{v}, \mathbf{v}_i). \quad (6)$$

In this formulation, each grid point \mathbf{r} has its own set of model weights $\beta(\mathbf{r})$, which means that we would need to train a separate model for each grid point of the density. Given the cubic growth of the potential and density grids, it is easy to see that this approach would quickly become intractable even for small molecules. Additionally, nearby grid-points are strongly correlated, and using independent models for nearby points would essentially disregard the information contained in the local correlations.

To circumvent this obvious drawback, we use a basis representation for the density of the form

$$n(\mathbf{r}) = \sum_{l=1}^L u^{(l)}\phi_l(\mathbf{r}), \quad (7)$$

where ϕ_l are basis functions and $u^{(l)}$ are the corresponding basis coefficients. Here we use the Fourier basis representation for the electron density, however many other basis representations such as kernel PCA[24] or atom-centered Gaussian type orbitals [28] can also be used. With this formulation, we can transform the learning problem from one of predicting the density grid points to one of predicting the basis coefficients $u^{(l)}[v]$, giving us the following model for the predicted density

$$n^{\text{ML}}[\mathbf{v}](\mathbf{r}) = \sum_{l=1}^L u^{(l)}[\mathbf{v}]\phi_l(\mathbf{r}). \quad (8)$$

Using KRR, the model for each coefficient can be formulated as

$$u^{\text{ML}(l)}[\mathbf{v}] = \sum_{i=1}^M \beta_i^{(l)}k(\mathbf{v}, \mathbf{v}_i), \quad (9)$$

with $\beta^{(l)}$ representing the model weights associated with each basis coefficient and k being the Gaussian kernel. The resulting contributions of the prediction error to the cost function are given by

$$\begin{aligned} \text{err}(\boldsymbol{\beta}) &= \sum_{i=1}^M \|n_i - n^{\text{ML}}[\mathbf{v}_i]\|_{\mathcal{L}_2}^2 \\ &= \sum_{i=1}^M \left\| n_i - \sum_{l=1}^L u^{\text{ML}(l)}[\mathbf{v}_i]\phi_l \right\|_{\mathcal{L}_2}^2. \end{aligned} \quad (10)$$

By writing the density in terms of its basis representation and assuming orthogonality of the basis functions we obtain

$$\begin{aligned}
err(\boldsymbol{\beta}) &= \sum_{i=1}^M \left\| \sum_{l=1}^L u_i^{(l)} \phi_l - \sum_{l=1}^L u^{\text{ML}(l)}[\mathbf{v}_i] \phi_l \right\|_{\mathcal{L}_2}^2 \\
&= \sum_{i=1}^M \left\| \sum_{l=1}^L \left(u_i^{(l)} - u^{\text{ML}(l)}[\mathbf{v}_i] \right) \phi_l \right\|_{\mathcal{L}_2}^2 \\
&= \sum_{i=1}^M \int \sum_{l=1}^L \left(u_i^{(l)} - u^{\text{ML}(l)}[\mathbf{v}_i] \right) \phi_l(\mathbf{r}) \sum_{l'=1}^L \left(u_i^{(l')} - u^{\text{ML}(l')}[\mathbf{v}_i] \right) \phi_{l'}^*(\mathbf{r}) d\mathbf{r} \\
&= \sum_{i=1}^M \sum_{l,l'=1}^L \left(u_i^{(l)} - u^{\text{ML}(l)}[\mathbf{v}_i] \right) \left(u_i^{(l')} - u^{\text{ML}(l')}[\mathbf{v}_i] \right) \int \phi_l(\mathbf{r}) \phi_{l'}^*(\mathbf{r}) d\mathbf{r} \\
&= \sum_{i=1}^M \sum_{l=1}^L \left(u_i^{(l)} - u^{\text{ML}(l)}[\mathbf{v}_i] \right)^2 \\
&= \sum_{i=1}^M \sum_{l=1}^L \left(u_i^{(l)} - \sum_{j=1}^M \beta_j^{(l)} k(\mathbf{v}_i, \mathbf{v}_j) \right)^2.
\end{aligned} \tag{11}$$

The resulting equation shows that the error can be decomposed into the independent error contributions for each of the basis coefficients. By viewing the errors independently we obtain L separate KRR minimization problems, and analogously to equations 2 and 3 we obtain the analytical solutions

$$\boldsymbol{\beta}^{(l)} = \left(\mathbf{K}_{\sigma^{(l)}} + \lambda^{(l)} \mathbf{I} \right)^{-1} \mathbf{u}^{(l)}, \quad l = 1, \dots, L, \tag{12}$$

where for each basis function ϕ_l , $\lambda^{(l)}$ is a regularization parameter, $\mathbf{u}^{(l)}$ is a vector containing the training set coefficients for the l -th basis function and $\mathbf{K}_{\sigma^{(l)}}$ is a Gaussian kernel matrix with width $\sigma^{(l)}$.

By independently and directly predicting the basis coefficients, the machine learning model becomes more efficient and easier to scale to larger molecules. Additionally, the basis representation allows us to use the predicted coefficients to reconstruct the continuous density at any point in space, making the predicted density independent of a fixed grid and enabling computations such as numerical integrals to be performed on the predicted density at an arbitrary accuracy.

Finally after the ML-HK map is learned, modelling the energy functional requires a single KRR model of the form

$$E^{ML}[n] = \sum_{i=1}^M \boldsymbol{\alpha}_i k(\mathbf{u}^{\text{ML}}[\mathbf{v}], \mathbf{u}^{\text{ML}}[\mathbf{v}_i]). \tag{13}$$

where $\mathbf{u}^{\text{ML}}[\mathbf{v}] = [u^{\text{ML}(1)}[\mathbf{v}], \dots, u^{\text{ML}(L)}[\mathbf{v}]]$ and k is once again the Gaussian kernel.

2.4 Cross-validation

All hyperparameters used in the model are estimated solely on the training set. The width γ and spacing Δ hyperparameters for the artificial Gaussians potential were optimized for all molecules at the same time, with the resulting optimal values being $\gamma = 0.2 \text{ \AA}$ and $\Delta = 0.08 \text{ \AA}$, while the kernel width σ and the regularization parameter λ were optimized individually for each molecule. In both cases the hyperparameter optimization was performed using cross-validation [8]. After training, the model is fixed and is applied unchanged on the out-of-sample test set.

2.5 Functional and density driven error

In order to more accurately measure the error of ML-HK map, we can separate out the effect of the error in the functional F and the error in the density $n(\mathbf{r})$ from the resulting error in the total

energy, as shown in [36]. Let \tilde{F} denote an approximation of the many body functional F , and $\tilde{n}(\mathbf{r})$ the resulting approximate ground-state density when \tilde{F} is used in the Euler equation. Defining $\tilde{E}[n] = \tilde{F}[n] + \int d^3r n(\mathbf{r}) v(\mathbf{r})$ yields

$$\Delta E = \tilde{E}[\tilde{n}] - E[n] = \Delta E_{\text{F}} + \Delta E_{\text{D}} \quad (14)$$

where $\Delta E_{\text{F}} = \tilde{F}[n] - F[n]$ is the functional-driven error, and $\Delta E_{\text{D}} = \tilde{E}[\tilde{n}] - \tilde{E}[n]$ is the density-driven error. We will use these additional error definitions to measure the accuracy of the ML-HK map.

2.6 Results

Here we revisit the results of applying the ML-HK map to predict electron densities and energies for a series of small 3D molecules. Using a set of test molecules, we compare the predictions of the ML model with the KS-DFT results obtained as described in Section 2.1. Additionally we compare the ML-HK map using the Fourier basis representation the approach of directly mapping from the potential grid $v(\mathbf{r})$ to the total energy. We call this approach the ML-KS model, with the resulting KRR formulation being

$$E^{\text{ML}}[v] = \sum_{i=1}^M \alpha_i k(v, v_i). \quad (15)$$

The first and most basic molecular prototypes used to evaluate the model were H_2 and H_2O , with the datasets being generated with one and three degrees of freedom respectively. For more details on the composition of the datasets see [24].

For the evaluation of the models, for both datasets a random sample of 50 molecules was taken as an out-of-sample test set. Additionally, for each of the molecules multiple subsets of varying sizes M were chosen out of the rest of the samples as training sets for both models.

	M	ML-KS		ML-HK			
		ΔE		ΔE		$\Delta E_{\text{D}}^{\text{ML}}$	
Molecule		MAE	max	MAE	max	MAE	max
H_2	5	1.3	4.3	0.70	2.9	0.18	0.54
	7	0.37	1.4	0.17	0.73	0.054	0.16
	10	0.080	0.41	0.019	0.11	0.017	0.086
H_2O	5	1.4	5.0	1.1	4.9	0.056	0.17
	10	0.27	0.93	0.12	0.39	0.099	0.59
	15	0.12	0.47	0.043	0.25	0.029	0.14
	20	0.015	0.064	0.0091	0.060	0.011	0.058

Table 1: **Prediction errors on H_2 and H_2O .** Shown for increasing number of training points M for the ML-KS and ML-HK approaches. In addition, the estimated density-driven contribution to the error for the ML-HK approach is given. In all cases except at maximum M , the energy error in the ML-HK map is largely is the energy map, not the density map. Energies are in kcal/mol.

Since the size of some training subsets is very small, careful selection of the samples is required in order to ensure that the subset covers the complete range of geometries. This is achieved via K-means sampling, which selects the M training points so that the samples are nearly equally spaced in the geometry space (see [24]).

The performance of the ML-KS map is evaluated by comparing predicted total energy $E^{\text{ML}}[v]$ that is mapped directly from the Gaussians potential with the calculated KS-DFT energies. For the ML-HK map the total energy $E^{\text{ML}}[n]$ is obtained by mapping from the predicted density $n^{\text{ML}}[v]$, which itself is predicted by mapping from the potential to the ground-state density in a three-dimensional

Fourier basis representation (using 25 basis functions for each dimension, for a total of 125000 basis coefficients).

Table 1 shows the resulting performance of the models when trained on datasets of varying sizes and evaluated using the out-of-sample test sets. The mean average error (MAE) of energy predicted using the ML-HK map is significantly smaller than that of the ML-KS map, indicating that learning the potential-to-density map and subsequently learning the density-to-energy functional is easier than directly learning the potential-to-energy map, at least when using our representations for the potential and density.

For H₂O, in order to achieve similar accuracies as for H₂ we need a larger training set, which is expected due to the increased degrees of freedom and complexity of the H₂O molecule. Considering that the MAE of PBE energies relative to CCSD(T) calculations is 1.2 kcal/mol for the water dataset, the additional error introduced by the predicted PBE energies using the ML-HK map is negligible.

For larger molecules, the number of degrees of freedom is much higher, making it difficult to randomly generate conformers that span the full configurational space. Therefore, large datasets of conformers for benzene, ethane and malonaldehyde were generated using classical force field molecular dynamics. The MD simulations were performed at 300 K, 350 K, and 400 K using the General Amber Force Field (GAFF)[37] in the PINY_MD package[38]. The MD simulations generate a large and varied set of geometries which are then sub-sampled using the K-means approach to obtain 2,000 points which constitute the training set for each of the molecules.

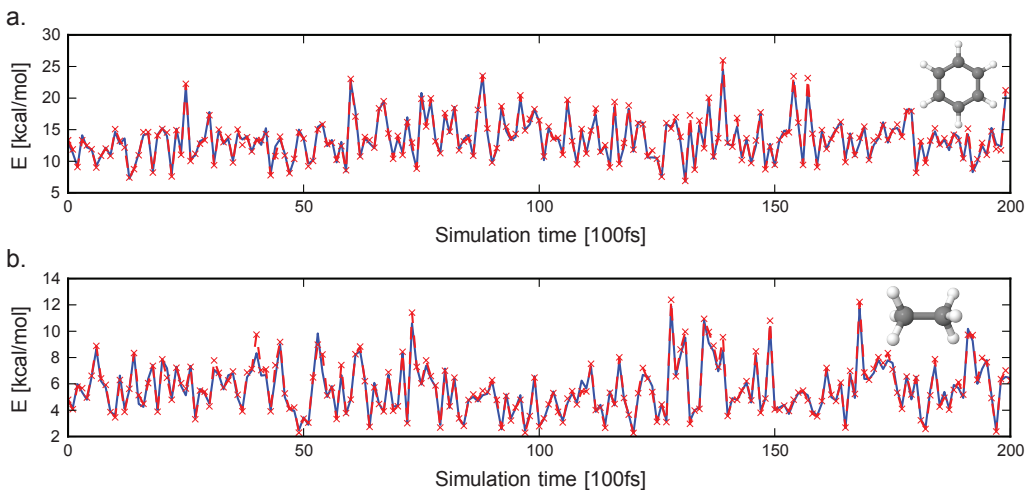


Figure 2: **Energy errors of ML-HK along classical MD trajectories.** PBE values in blue, ML-HK values in red. **a.** A 20 ps classical trajectory of benzene. **b.** A 20 ps classical trajectory of ethane. Figure adapted from Brockherde et al. [24].

The training for the ML-HK and ML-KS models is performed as described above using reference KS-DFT calculations for the density and total energy for a training set size of $M = 2000$ points. The performance of each models is then tested on random samples taken from independent trajectories run at 300 K. Additionally, the performance is evaluated for training sets composed of combined samples from MD trajectories at 300 K and a higher temperature, since this should increase the span of the training set geometries, resulting in better generalization. The results of the evaluations for all three molecules are shown on Table 2.

The MAE achieved on the test snapshots using the ML-HK map trained on a set of 2000 samples is consistently under 1 kcal/mol for each of the molecules. Additionally, learning from a training set combining samples from trajectories run at higher temperatures improves the performance, however, which higher temperature brings the largest benefits depends on the molecule itself. Figure 2 visualizes the differences between the energies from the ML-HK map and the KS-DFT calculations on the test sets for benzene and ethane. The versatility of the ML-HK map is further demonstrated by

Molecule	Training tra- jectories	ΔE		ΔE_D^{ML}	
		MAE	max	MAE	max
Benzene	300K	0.42	1.7	0.32	1.5
	300K + 350K	0.37	1.8	0.28	1.5
	300K + 400K	0.47	2.3	0.30	1.8
Ethane	300K	0.20	1.5	0.17	1.3
	300K + 350K	0.23	1.4	0.19	1.1
	300K + 400K	0.14	1.7	0.098	0.62
Malonaldehyde	300K + 350K	0.27	1.2	0.21	0.74

Table 2: **Energy and density-driven errors of the ML-HK approach on the MD datasets.** Errors are given in kcal/mol for different training trajectory combinations.

Figure 3a, where the model manages to interpolate the energies for a proton transfer in malonaldehyde, even though such geometries were not generated by the classical force field MD and thus were not present in the training set.

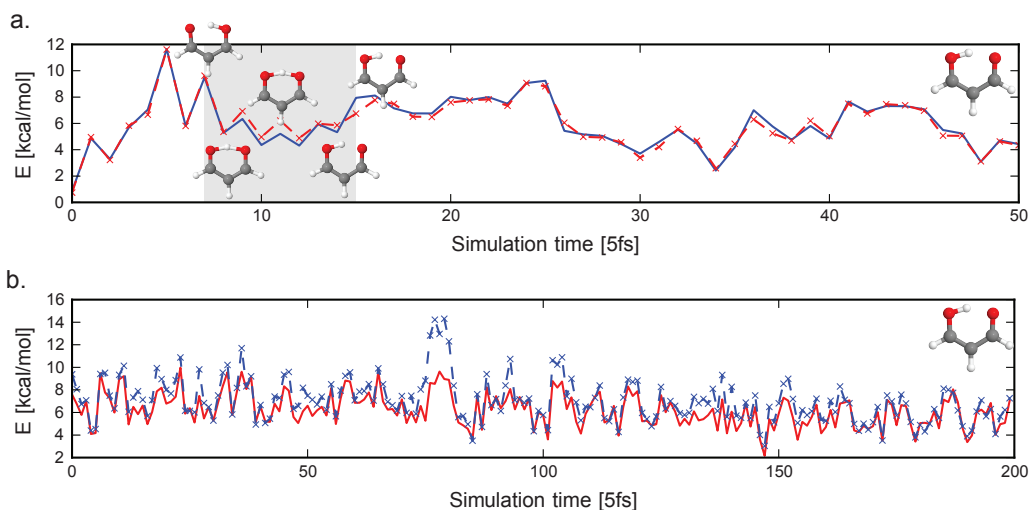


Figure 3: **Energy errors of ML-HK along ab-initio MD and ML generated trajectories.** **a.** Energy errors of ML-HK along a 0.25 ps ab initio MD trajectory of malonaldehyde. PBE values in blue, ML-HK values in red. The ML model correctly predicts energies during a proton transfer in frames 7 to 15 without explicitly including these geometries in the training set. **b.** Energy errors of ML-HK along a 1 ps MD trajectory of malonaldehyde generated by the ML-HK model. ML-HK values in red, PBE values of trajectory snapshots in blue. Figure adapted from Brockherde et al. [24].

Finally, the ML-HK map for malonaldehyde can also be used to generate an MD trajectory at 300 K, obtained by finite-difference approach to determine the atomic forces from the predicted energies (see Figure 3b). Despite some molecular configurations where the energy is underestimated (maximum absolute error of 5.7 kcal/mol), the resulting forces are still large enough to bring the molecule to the equilibrium, resulting in a stable trajectory. Being able to run MD simulations using the ML-HK map can greatly reduce the computation effort compared to running MD simulations with DFT, while at the same time providing results that are very close to DFT accuracy. It is important to note that there are multiple ML models capable of providing even more accurate MD simulations by directly

learning the force field [14, 17, 16, 19–21, 11], however this experiment demonstrates that stable MD simulations can also be produced using a force free machine learning model.

3 Discussion

The work revisited in this submission was one of the first ML models capable of efficiently and accurately predicting both the electron density and total energy of small atomistic systems. While there are many machine learning models that directly predict the total energy with greater accuracy, predicting the density as an intermediate step opens up many different possibilities, such as using the density as an universal descriptor to predict other properties (due to the Hohenberg-Kohn theorem[1]) or plugging the predicted density directly into DFT codes to perform calculations.

Here we showed once again in more detail how the problem of modelling a 3D electron density can be simplified by using a basis representation and learning to predict the basis coefficients, and how for orthogonal basis functions problem of predicting the coefficients can be decomposed into independent learning problems for each of the coefficients. This greatly improves the simplicity and efficiency of the resulting machine learning model.

Since the model is not dependent on the reference calculations used for training, the ML-HK map can be trained using electron densities obtained by other methods besides KS-DFT, such as Hartree-Fock or even CCSD densities. The same holds for the energy functional map, giving us the possibility of predicting total energies using electron densities obtained using different levels of theory, potentially leading to even larger gains in computational efficiency.

There is also plenty of room for improvement of the current model in the future. One of the main challenges of the current model is its handling of the many symmetries in the data. While the potential used as a descriptor is invariant to permutational symmetries, rotational symmetries have to be explicitly tackled by rotating each of the molecules to optimally align with a reference geometry, which can often be a source of noise, since the conformers often do not perfectly match the reference. Additionally, the current descriptor has no way to handle mirror symmetries, meaning that the model would require a larger number of training samples to learn these symmetries. The same holds for the Fourier basis representation, which is also not invariant to symmetries of the $O(3)$ group. Consequently, an obvious avenue for improvement would be to incorporate descriptors that are invariant to the various symmetries, both for the atomistic systems [39, 6, 40] and the electron densities [41].

Finally, since the ML-HK map is independent from the subsequent density-to-energy map, the model can be easily extended to predict various other properties of the atomistic system, for example by replacing the density-to-energy map by a density-to-forces map, which has the potential of drastically improving the accuracy the MD simulations produced using the machine learning model.

This demonstrates the flexibility of the formulation of the ML-HK map and provides many potential directions in which the results discussed here can be further expanded and improved.

4 Acknowledgments

We thank IPAM at UCLA for repeated hospitality. Work at UC Irvine supported by NSF CHE-1464795. KRM and FB thank the Einstein Foundation for generously funding the ETERNAL project. This research was supported by Institute for Information & Communications Technology Promotion and funded by the Korea government (MSIT) (No. 2017-0-00451, No. 2017-0-01779). Work at NYU supported by the U.S. Army Research Office under contract/grant number W911NF-13-1-0387 (MET and LV). Ab initio trajectory was run using High Performance Computing resources at NYU. Other DFT simulations were run using High Performance Computing resources at MPI Halle.

References

- [1] Pierre Hohenberg and Walter Kohn. Inhomogeneous electron gas. *Physical review*, 136(3B):B864, 1964.
- [2] Walter Kohn and Lu Jeu Sham. Self-consistent equations including exchange and correlation effects. *Physical review*, 140(4A):A1133, 1965.

- [3] Aurora Pribram-Jones, David A Gross, and Kieron Burke. DFT: A theory full of holes? *Annual review of physical chemistry*, 66:283–304, 2015.
- [4] Matthias Rupp, O. Anatole von Lilienfeld, and Kieron Burke. Guest editorial: Special topic on data-enabled theoretical chemistry. *The Journal of Chemical Physics*, 148(24):241401, 2018.
- [5] Matthias Rupp, Alexandre Tkatchenko, Klaus-Robert Müller, and O Anatole Von Lilienfeld. Fast and accurate modeling of molecular atomization energies with machine learning. *Physical review letters*, 108(5):058301, 2012.
- [6] Sandip De, Albert P Bartók, Gábor Csányi, and Michele Ceriotti. Comparing molecules and solids across structural and alchemical space. *Physical Chemistry Chemical Physics*, 18(20):13754–13769, 2016.
- [7] KV Jovan Jose, Nongnuch Artrith, and Jörg Behler. Construction of high-dimensional neural network potentials using environment-dependent atom pairs. *The Journal of chemical physics*, 136(19):194111, 2012.
- [8] Katja Hansen, Grégoire Montavon, Franziska Biegler, Siamac Fazli, Matthias Rupp, Matthias Scheffler, O Anatole Von Lilienfeld, Alexandre Tkatchenko, and Klaus-Robert Müller. Assessment and validation of machine learning methods for predicting molecular atomization energies. *Journal of Chemical Theory and Computation*, 9(8):3404–3419, 2013.
- [9] Kristof T Schütt, Farhad Arbabzadah, Stefan Chmiela, Klaus R Müller, and Alexandre Tkatchenko. Quantum-chemical insights from deep tensor neural networks. *Nature communications*, 8:13890, 2017.
- [10] Felix A Faber, Luke Hutchison, Bing Huang, Justin Gilmer, Samuel S Schoenholz, George E Dahl, Oriol Vinyals, Steven Kearnes, Patrick F Riley, and O Anatole von Lilienfeld. Prediction errors of molecular machine learning models lower than hybrid DFT error. *Journal of chemical theory and computation*, 13(11):5255–5264, 2017.
- [11] Kristof Schütt, Pieter-Jan Kindermans, Huziel Enoc Saucedo Felix, Stefan Chmiela, Alexandre Tkatchenko, and Klaus-Robert Müller. Schnet: A continuous-filter convolutional neural network for modeling quantum interactions. In *Advances in Neural Information Processing Systems*, pages 991–1001, 2017.
- [12] Wiktor Pronobis, Alexandre Tkatchenko, and Klaus-Robert Müller. Many-body descriptors for predicting molecular properties with machine learning: Analysis of pairwise and three-body interactions in molecules. *Journal of chemical theory and computation*, 2018.
- [13] Kun Yao, John E Herr, David W Toth, Ryker Mckintyre, and John Parkhill. The tensormol-0.1 model chemistry: a neural network augmented with long-range physics. *Chemical science*, 9(8):2261–2269, 2018.
- [14] Stefan Chmiela, Alexandre Tkatchenko, Huziel E Saucedo, Igor Poltavsky, Kristof T Schütt, and Klaus-Robert Müller. Machine learning of accurate energy-conserving molecular force fields. *Science advances*, 3(5):e1603015, 2017.
- [15] Zhenwei Li, James R Kermode, and Alessandro De Vita. Molecular dynamics with on-the-fly machine learning of quantum-mechanical forces. *Physical review letters*, 114(9):096405, 2015.
- [16] Andrea Grisafi, David M Wilkins, Gábor Csányi, and Michele Ceriotti. Symmetry-adapted machine learning for tensorial properties of atomistic systems. *Physical review letters*, 120(3):036002, 2018.
- [17] Stefan Chmiela, Huziel E Saucedo, Klaus-Robert Müller, and Alexandre Tkatchenko. Towards exact molecular dynamics simulations with machine-learned force fields. *arXiv preprint arXiv:1802.09238*, 2018.
- [18] Michael Gastegger, Jörg Behler, and Philipp Marquetand. Machine learning molecular dynamics for the simulation of infrared spectra. *Chemical science*, 8(10):6924–6935, 2017.

- [19] Aldo Glielmo, Claudio Zeni, and Alessandro De Vita. Efficient nonparametric n-body force fields from machine learning. *Physical Review B*, 97(18):184307, 2018.
- [20] Linfeng Zhang, Jiequn Han, Han Wang, Roberto Car, and E Weinan. Deep potential molecular dynamics: a scalable model with the accuracy of quantum mechanics. *Physical review letters*, 120(14):143001, 2018.
- [21] Anders S Christensen, Felix A Faber, and O Anatole von Lilienfeld. Operators in machine learning: Response properties in chemical space. *arXiv preprint arXiv:1807.08811*, 2018.
- [22] John C Snyder, Matthias Rupp, Katja Hansen, Klaus-Robert Müller, and Kieron Burke. Finding density functionals with machine learning. *Physical review letters*, 108(25):253002, 2012.
- [23] Li Li, Thomas E Baker, Steven R White, Kieron Burke, et al. Pure density functional for strong correlation and the thermodynamic limit from machine learning. *Physical Review B*, 94(24):245129, 2016.
- [24] Felix Brockherde, Leslie Vogt, Li Li, Mark E Tuckerman, Kieron Burke, and Klaus-Robert Müller. Bypassing the kohn-sham equations with machine learning. *Nature communications*, 8(1):872, 2017.
- [25] Junji Seino, Ryo Kageyama, Mikito Fujinami, Yasuhiro Ikabata, and Hiromi Nakai. Semi-local machine-learned kinetic energy density functional with third-order gradients of electron density. *The Journal of Chemical Physics*, 148(24):241705, 2018.
- [26] Matthew Welborn, Lixue Cheng, and Thomas F. Miller. Transferability in machine learning for electronic structure via the molecular orbital basis. *Journal of Chemical Theory and Computation*, 14(9):4772–4779, 2018.
- [27] Anton V. Sinitskiy and Vijay S. Pande. Deep neural network computes electron densities and energies of a large set of organic molecules faster than density functional theory (dft). *arXiv preprint arXiv:1809.02723*, 2018.
- [28] Andrea Grisafi, David M Wilkins, Benjamin AR Meyer, Alberto Fabrizio, Clemence Corminboeuf, and Michele Ceriotti. A transferable machine-learning model of the electron density. *arXiv preprint arXiv:1809.05349*, 2018.
- [29] Paolo Giannozzi, Stefano Baroni, Nicola Bonini, Matteo Calandra, Roberto Car, Carlo Cavazzoni, Davide Ceresoli, Guido L Chiarotti, Matteo Cococcioni, Ismaila Dabo, Andrea Dal Corso, Stefano de Gironcoli, Stefano Fabris, Guido Fratesi, Ralph Gebauer, Uwe Gerstmann, Christos Gougoussis, Anton Kokalj, Michele Lazzeri, Layla Martin-Samos, Nicola Marzari, Francesco Mauri, Riccardo Mazzarello, Stefano Paolini, Alfredo Pasquarello, Lorenzo Paulatto, Carlo Sbraccia, Sandro Scandolo, Gabriele Sclauzero, Ari P Seitsonen, Alexander Smogunov, Paolo Umari, and Renata M Wentzcovitch. Quantum espresso: a modular and open-source software project for quantum simulations of materials. *Journal of Physics: Condensed Matter*, 21(39):395502 (19pp), 2009.
- [30] John P Perdew, Kieron Burke, and Matthias Ernzerhof. Generalized gradient approximation made simple. *Physical review letters*, 77(18):3865, 1996.
- [31] Georg Kresse and D Joubert. From ultrasoft pseudopotentials to the projector augmented-wave method. *Physical Review B*, 59(3):1758, 1999.
- [32] Peter E Blöchl. Projector augmented-wave method. *Physical review B*, 50(24):17953, 1994.
- [33] Norman Troullier and José Luís Martins. Efficient pseudopotentials for plane-wave calculations. *Physical review B*, 43(3):1993, 1991.
- [34] Trevor Hastie, Robert Tibshirani, and JH Friedman. The elements of statistical learning: data mining, inference, and prediction, 2009.
- [35] John C Snyder, Sebastian Mika, Kieron Burke, and Klaus-Robert Müller. Kernels, pre-images and optimization. In *Empirical Inference*, pages 245–259. Springer, 2013.

- [36] Min-Cheol Kim, Eunji Sim, and Kieron Burke. Understanding and reducing errors in density functional calculations. *Physical review letters*, 111(7):073003, 2013.
- [37] Junmei Wang, Romain M Wolf, James W Caldwell, Peter A Kollman, and David A Case. Development and testing of a general amber force field. *Journal of computational chemistry*, 25(9):1157–1174, 2004.
- [38] Mark E Tuckerman, DA Yarne, Shane O Samuelson, Adam L Hughes, and Glenn J Martyna. Exploiting multiple levels of parallelism in molecular dynamics based calculations via modern techniques and software paradigms on distributed memory computers. *Computer Physics Communications*, 128(1-2):333–376, 2000.
- [39] KT Schütt, H Glawe, F Brockherde, A Sanna, KR Müller, and EKV Gross. How to represent crystal structures for machine learning: Towards fast prediction of electronic properties. *Physical Review B*, 89(20):205118, 2014.
- [40] Felix A Faber, Anders S Christensen, Bing Huang, and O Anatole von Lilienfeld. Alchemical and structural distribution based representation for universal quantum machine learning. *The Journal of Chemical Physics*, 148(24):241717, 2018.
- [41] Michael Eickenberg, Georgios Exarchakis, Matthew Hirn, Stéphane Mallat, and Louis Thiry. Solid harmonic wavelet scattering for predictions of molecule properties. *The Journal of Chemical Physics*, 148(24):241732, 2018.